Proceedings of the 21st ICSMGE, Vienna, Austria, 14 – 19 June 2026. Pistrol, Adam & Schweiger (eds.)
Published by: ÖGG, Austrian Society for Geomechanics, Salzburg, Austria, ISBN 978-3-9503898-4-5
https://doi.org/10.53243/ICSMGE2026-2333

Development of 3D structural filter for sandy soil

Yukio Nakata, Yoko Ohta
Department of Civil and Environmental Engineering, Yamaguchi University, Ube, Japan, nakata@yamaguchi-u.ac.jp

Jun Yoneda
National Institute of Advanced Industrial Science and Technology, Sapporo, Japan

ABSTRACT: In geotechnical engineering, filters are essential for preventing soil particle migration while maintaining adequate permeability. They are widely used in coastal structures, drainage systems, and embankments. However, filter clogging has become a growing concern due to intensified rainfall and evolving weather patterns. Clogging can form impermeable layers, elevate pore water pressure, and increase the risk of slope failure. Matching the filter's pore size to the surrounding soil's grain size is essential, but conventional solutions such as naturally occurring soils or geotextiles often lack the flexibility to accommodate diverse soil conditions. This study investigates the applicability and design criteria of a three-dimensional (3D) structural filter, which allows precise customization of filter geometry to match the grain size of the surrounding soil. Two types of experiments were conducted: a small-scale seepage failure test using embankment models, and a one-dimensional permeability test to evaluate the structural properties of the 3D filter. In the embankment tests, diamond and gyroid 3D filters were used as horizontal drainage layers. The results showed that the filters effectively prevented failure and reduced internal water head, performing comparably to silica sand filters. Clogging was minimized, and permeability was maintained when the filter's pore diameter was less than 10 times the D_{15}^{s} of the soil. In the permeability tests, filters with varying wire diameters were evaluated using glass beads. The results indicated that particle intrusion was minimized when the wire diameter ranged between 5 and 10 times the D_{15}^{s} of the soil. These findings suggest that 3D filters can be an effective and adaptable solution for drainage and filtration in geotechnical applications, offering a balance between structural stability and anti-clogging performance.

KEYWORDS: Geotechnical filter, filter criterion, 3D structure, clogging, seepage test.

1 INTRODUCTION

In geotechnical engineering, filters are installed to prevent the movement of soil particles—particularly fine particles—while maintaining adequate permeability. This concept originated with its application to rockfill dams (Terzaghi, 1926) and has since been adopted in various structures. For example, filters are used to prevent suction behind retaining walls in coastal structures behind breakwaters (Kudai et al., 2021), and to prevent the flow fines out around perforated pipes buried in embankments for drainage or for collecting water within slopes (Fujiwara et al., 2020). As the applications of filters have expanded, one critical issue that has emerged is the reduction in permeability due to clogging. When clogging occurs such as within embankments an impermeable layer may form internally, which can lead to an increase in water head and, in severe cases, significant deformation.

Preventing and mitigating filter clogging has become increasingly important due to intensified rainfall and changing precipitation patterns. A key strategy to address this issue is to design the filter to match the grain size distribution of the original soil. Recent studies have investigated the use of geotextiles and multi-layer soil filters, primarily utilizing standardized filter materials or naturally occurring soils. However, to effectively solve clogging across diverse soil conditions, there is a need for filters that can be custom-designed to suit the specific grain size characteristics of the original soil material.

A three-dimensional structural filter, such as a cubic lattice structure, is a promising solution. It is a grid-type filter with a customizable 3D configuration that can be tailored to the grain size of the original soil, making it an achievable alternative to conventional filter materials.

Therefore, this study aims to collect foundational data to evaluate the applicability of 3D structural filters and to explore their design criteria. This paper presents the results of small-scale embankment seepage failure experiments conducted to assess the feasibility of the proposed 3D filters, along with one-dimensional seepage tests aimed at investigating their structural characteristics.

2 3D STRUCTURAL FILTER

The structure of a three-dimensional (3D) filter is defined by two key parameters: the gap diameter (d), which represents the size of the pore space within the grid, and the wire diameter (ϕ), which is the diameter of the structural elements forming the grid. In comparison to a conventional gravel filter, the pore diameter d of the 3D filter corresponds to the pore size of the gravel filter, while the wire diameter ϕ corresponds to the grain size D of the gravel particles. Unlike gravel filters, in which pore and particle sizes are inherently linked, the 3D filter allows d and ϕ to be set independently, enabling more precise control over filtration performance.

In this study, we focused on diamond structures and gyroid triply periodic minimal surface structures (gyroid structures) (Schoen, 1970), due to their geometric symmetry and favorable mechanical properties, as illustrated in Figures 1 and 2. The diamond structure consists of two interlaced face-centered cubic lattices, offset by one-quarter of the lattice constant. Three design variations of the diamond structure were used, with the following combinations of gap diameter d and wire diameter ϕ:

d = 0.64 mm, ϕ = 0.26 mm
d = 1.27 mm, ϕ = 0.52 mm
d = 1.88 mm, ϕ = 0.76 mm

The gyroid structure is known for its superior rigidity and compressive strength compared to other lattice types (Nguyen-Van et al., 2020; Al-Ketan et al., 2018). In this study, three gyroid configurations were employed, with the following gap diameters d: 0.83 mm, 1.64 mm, and 2.44 mm. The wire diameter ϕ of each configuration varies within a range, as follows:

d = 0.83 mm: ϕ ranges from 0.3 mm to 1.03 mm

d = 1.64 mm: ϕ ranges from 0.59 mm to 2.03 mm
d = 2.44 mm: ϕ ranges from 0.9 mm to 3.08 mm

This type of porous structure exhibits both mechanical strength and fluid dynamic performance. It has been applied in coastal engineering, such as in floating porous breakwaters and reinforced concrete structures (Dang et al., 2022).

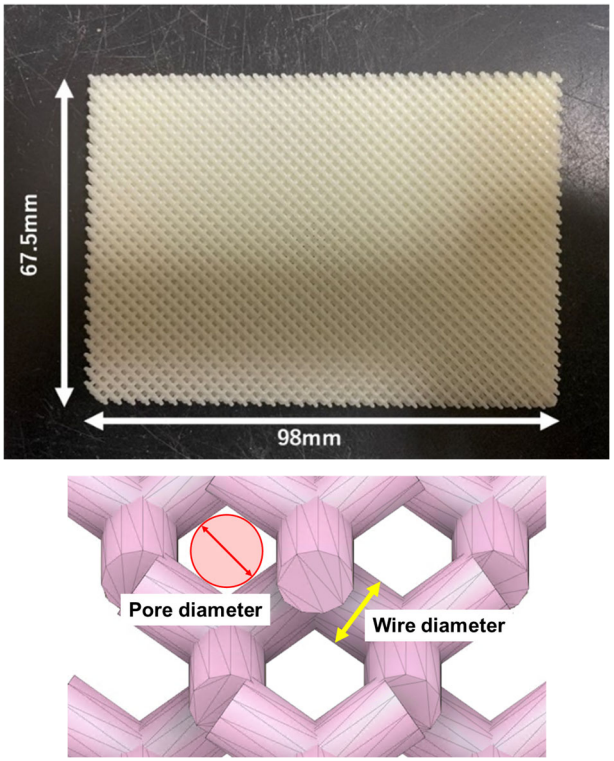

Figure 1. Diamond structure filter used.

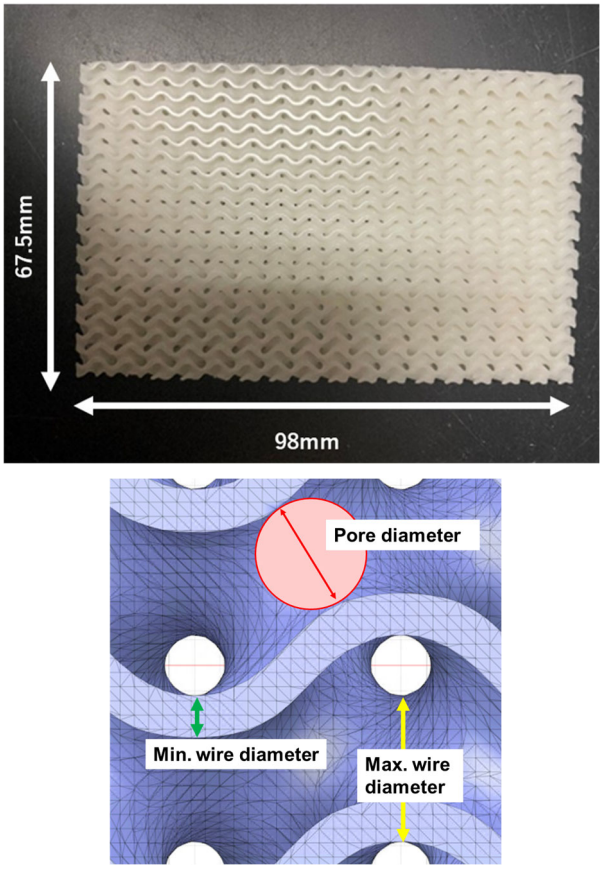

Figure 2. Gyroid structure filter used.

3 SEEPAGE MODEL TEST FOR EMBANKMENT

Figure 3 shows a schematic diagram of the seepage failure test apparatus used with the small-scale embankment model. The internal dimensions of the acrylic-walled container are 330 mm in width, 200 mm in height, and 100 mm in depth. The embankment model was constructed with a slope of 1:1.8, a crest width of 60 mm, an embankment height of 150 mm, and a base height of 50 mm.

A horizontal drainage layer was installed at the base of the embankment slope, measuring 135 mm in length and 5 mm in thickness. Three types of three-dimensional structural filters with different pore sizes were used as the drainage layer, each based on the aforementioned diamond and gyroid structures. The external dimensions of each 3D structural filter were 67.5 mm × 5 mm × 98 mm (as shown in Figures 1 and 2), and two filters were installed side by side. For comparison purposes, Ube silica sand.

Seepage was introduced from the right side of the embankment, with the water head controlled via the right-hand tank. Infiltration into the embankment occurred through the perforated plate, ranging from the base to a height of 150 mm, with a constant head of 240 mm. The duration of the seepage test was 24 hours (1,440 minutes). The outflow at the toe of the embankment was measured hourly for the first 5 hours and again at the 24-hour mark. The internal water head within the embankment was monitored using manometers No. 1 through No. 5, positioned at distances of 30 mm, 80 mm, 130 mm, 180 mm, 230 mm, and 280 mm from the toe (as shown in Figure 3). The horizontal drainage layer (i.e., the 3D filter) was installed above manometers No. 1 through No. 3.

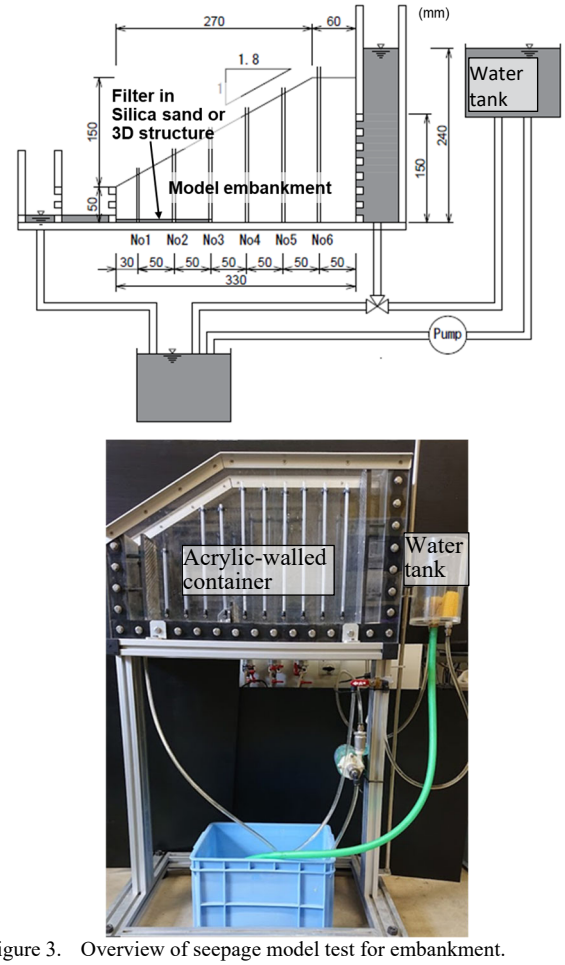

Figure 3. Overview of seepage model test for embankment.

The embankment soil used in the experiment was decomposed granite soil (referred to hereafter as Iwakuni Masado), with a particle density of 2.633 g/cm³. The grain size distribution of this soil, as shown in Figure 4 is characterised by: D_{15}^{s} = 0.065mm, D_{50}^{s} = 0.88mm, D_{85}^{s} = 3.0mm, and the uniformity coefficient is 95.5. The embankment was compacted using Iwakuni Masado at an optimal moisture content of 15.2% to achieve a dry density of 1.580 g/cm³ and a compaction ratio of 90.0%. Figure 4 also presents the grain size distribution of the Ube silica sand used as a conventional filter material. For this sand, $D_{15}{}^{f}$ = 2.52 mm. The dashed lines in the figure indicate the standard filter criteria established for rockfill dams, defined as:

$$\frac{D_{15}^{f}}{D_{15}^{s}} > 5, \quad \frac{D_{15}^{f}}{D_{85}^{s}} < 5 \tag{1}$$

Here, $D_{15}^{f}{}^{f}$ is the 15% particle size of the filter, and D_{15}^{s} and D_{85}^{s} are the 15% and 85% particle sizes of the base soil, respectively. For Iwakuni Masado, this implies that a suitable D_{15}^{f} value should range between approximately 0.33 mm and 15.0 mm. The D_{15}^{f} value of the silica sand used is logarithmically close to the midpoint of this range.

The relationship between grain size and pore size is given by the following empirical equation (Haverkamp and Parlange 1986):

$$d = \beta_r \, D \tag{2}$$

Here, β_r ranges from 0.2 to 0.4. If D is D_{15}^{f}, Equation (1) can be restated in terms of gap diameter d as:

$$(1\sim2)\, D_{15}^{s} < d < (1\sim2)\, D_{85}^{s} \tag{3}$$

Based on the D_{15}^{s} and D_{85}^{s} values for Iwakuni Masado, the allowable range for the gap diameter d is from 0.065 mm to 6 mm.

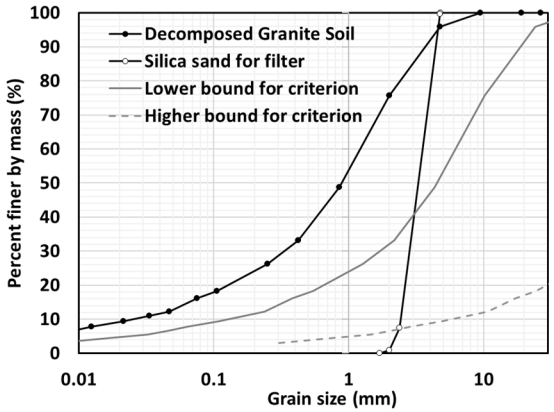

Figure 4. Particle size distribution for decomposed granite soil and silica sand.

Figure 5 shows the relationship between flow rate and elapsed time in the small-scale model embankment experiment. When no horizontal drainage layer was installed on the small model embankment, it collapsed 474 minutes after the start of the experiment. On the other hand, when any horizontal drainage layer was installed, the small-scale model embankment did not collapse or suffer any minor deformation until the end of the experiment.

When the silica sand filter was installed as the horizontal drainage layer, the flow rate decreased during first 5 hours and then slightly increased towards the end of the experiment. A similar trend was observed when the diamond structure filter was used. In contrast, the gyroid structure filter consistently showed a flow rate approximately 30 ml/min lower than the other filters.

Figure 6 presents the relationship between flow rate and pore size at the end of the experiment. The diamond structure filter exhibited a flow rate comparable to that of the silica sand filter. However, the gyroid structure filters with pore sizes of 0.8 mm and 1.6 mm showed lower flow rates than the diamond structure filter. This indicates that the flow rate is strongly influenced by the pore size in the gyroid structure filter.

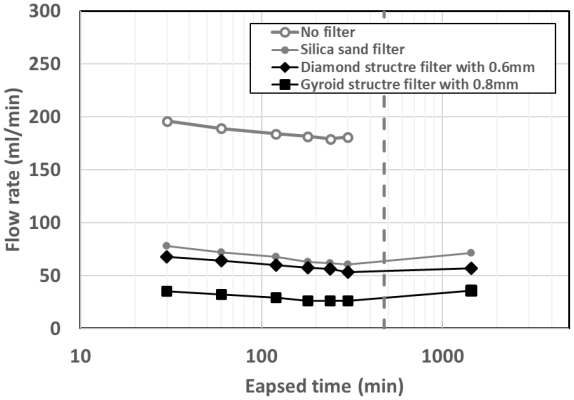

Figure 5. Time history of flow rate for seepage model test.

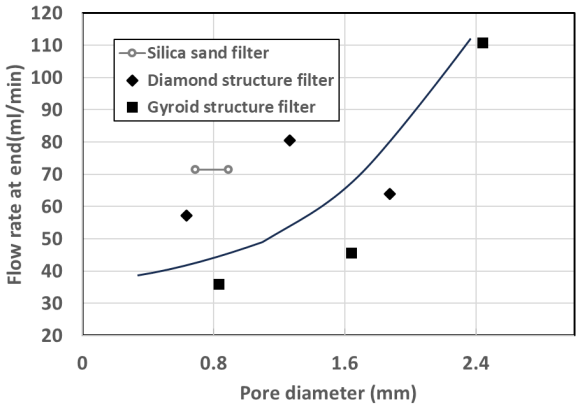

Figure 6. Effect of pore diameter on flow rate at the end of test.

Figure 7 compares the water head conditions at the final stage of the experiment. In the case without a horizontal drainage layer, the water head exceeded the slope surface at all manometer locations (No. 1 to No. 6), with the largest increase observed between No. 1 and No. 2. The collapse that occurred after 474 minutes was located near the No. 2 position. When the silica sand filter was installed, the rise in water head at manometers No. 1 to No. 3 was completely suppressed. The water head at manometers No. 4 to No. 6 was also lower compared to the case without a filter. Notably, a large head difference of 114.1 mm was observed between No. 3 and No. 4 at the end of the experiment.

With the 0.6 mm diamond structure filter, the water head distribution closely resembled that of the silica sand filter, with a final head difference of 113.4 mm between No. 3 and No. 4.

When the 0.8 mm gyroid structure filter was used, similar suppression of head rise at the toe of the slope was observed. A significant head difference of 150.6 mm was recorded between No. 3 and No. 4 at the end.

Figure 8 shows the relationship between the water head and the ratio of pore size to D_{15}^{s} at manometer No. 4 at the end of the experiment. The diamond structure filter consistently exhibited lower heads than the gyroid structure filter. Furthermore, smaller pore sizes correlated with lower water heads, and the 0.6 mm diamond structure filter resulted in a water head nearly identical to that of the silica sand filter. These results suggest that a pore size d of less than $10 \cdot D_{15}^{s}$ is appropriate. Based on this, the allowable range of pore sizes given in Equation (3) can be refined as:

$$D_{15}^{s} < d < 10D_{15}^{s} \quad (4)$$

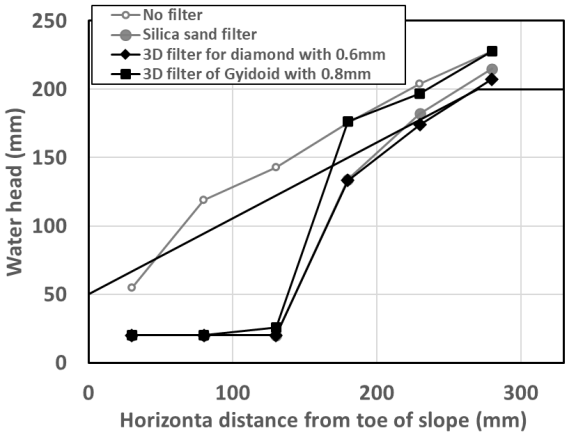

Figure 7. Water head at end of seepage model test.

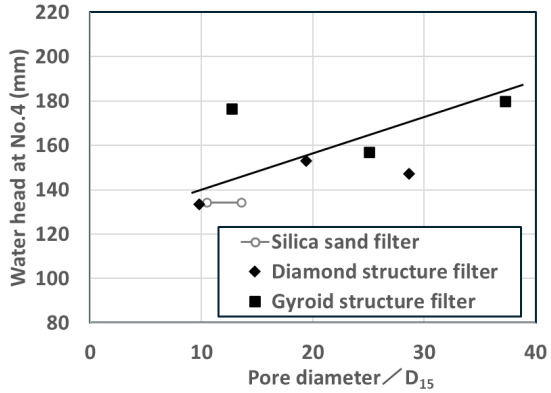

Figure 8. Final water head at No.4 plotted against normalised pore diameter.

After the experiment, X-ray CT imaging was used to analyze the internal condition of the 3D filters and quantify the amount of soil particles retained within them. Figures 9 and 10 show CT images of the 3D filters at the end of the experiment shown in Figure 7. The left images represent the filters on the front side of the slope, while the right images show those near the center. In the CT images, the 3D filter material appears light gray, and the soil particles are indicated in white.

Figure 11 presents the change in porosity, calculated from the total volume of retained particles inside the filters based on the CT data. The graph shows the relationship between porosity and water head at manometer No. 4 after 1 hour and 24 hours. The porosity before the experiment is the same as the porosity for the 3D filter, and the porosity after 24 hours represents the percentage of open space excluding the filter material and retained particles.

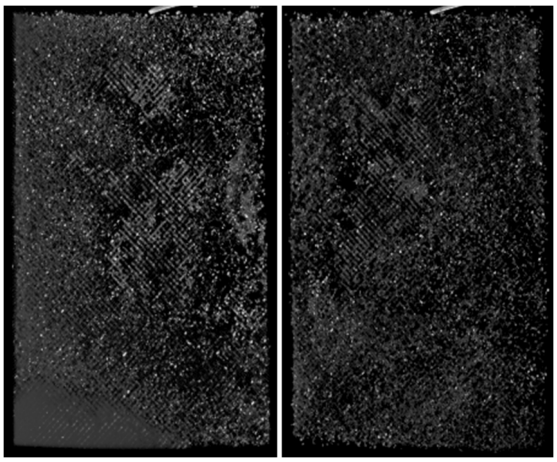

Figure 9. CT image after test for diamond filter with 0.6mm of pore diameter.

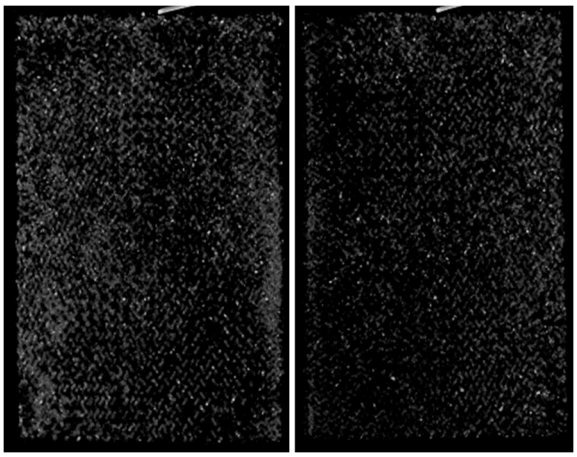

Figure 10. CT image after test for gyroid filter with 0.8mm of pore diameter.

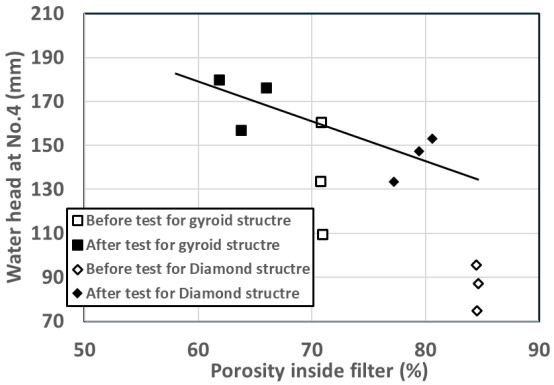

Figure 11. Variation of final water head at No.4 on porosity inside filter.

The diamond structure filter initially had a high porosity of 84%, and even after 24 hours, it maintained a porosity of around 80%. This small change suggests that clogging was minimal, allowing for stable head conditions and sustained drainage performance. Additionally, filters with smaller pore sizes

tended to resist clogging more effectively and maintained their original porosity.

In contrast, the gyroid structure filters used in this study had larger wire diameters than the diamond structures, resulting in lower initial porosity. As a consequence, they experienced more clogging during the experiment, leading to higher water heads. This indicates that the performance difference is not necessarily due to the gyroid geometry itself, but rather due to the specific wire diameter design used. Thus, optimizing the wire diameter is essential when designing 3D structural filters, regardless of the lattice type.

4 ONE-DIMENSIONAL PERMEABILITY EXPERIMENT FOR STRUCTURAL STANDARDS OF 3D FILTERS

To investigate the influence of wire diameter (ϕ) on the performance of 3D filters, a simplified one-dimensional seepage experiment was conducted using filters with a diamond lattice structure. Figure 10 illustrates the experimental setup, where disk-shaped 3D filters (150 mm in diameter) were placed in a vertical column. Four types of filters were fabricated, all with a fixed pore diameter (d) of 1.6 mm, but with different wire diameters: 1.6 mm, 2.4 mm, 3.2 mm, and 4.8 mm. Because each filter was composed of a single lattice structure, the resulting thicknesses varied from 93 mm to 193 mm, depending on the wire diameter.

The test samples used were glass beads with average particle sizes of 0.46 mm and 0.68 mm, referred to hereafter as GB-I and GB-II, respectively. The resulting pore size ratios, d/D_{15}^{s}, were 4.3 for GB-I and 2.7 for GB-II. Each specimen was compacted to achieve a porosity of 40%. A constant hydraulic head of 600 mm was applied, and continuous seepage was maintained for 24 hours. Across all test conditions, no significant variation in flow rate was observed during the experiment.

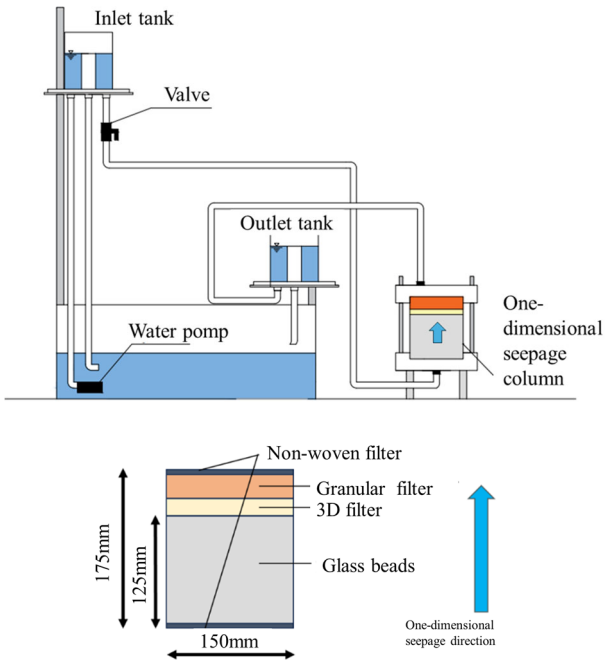

Figure 12. Overview of 1D seepage test with 3D structure filter.

After the test, the quantity of glass beads that had leaked through the 3D filter was measured. Figures 13 and 14 present photographs of the upper part of the filter with a wire diameter of 4.8 mm after the experiment. The image for GB-I clearly shows that the finer glass beads had leaked out the upper portion of the 3D filter.

Figure 13. Image for upper part of the 3D filter with 4.8mm wire diameter for GB-I.

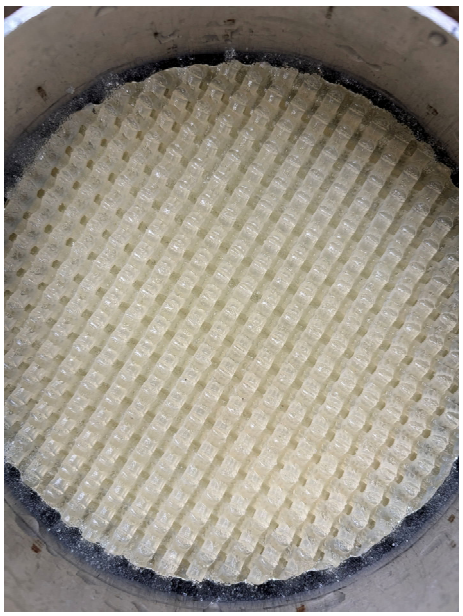

Figure 14. Image for upper part of the 3D filter with 4.8mm wire diameter for GB-II.

Figure 15 presents the relationships between wire diameter and (a) initial porosity of the filter, and (b) outflow volume. As wire diameter increased, initial porosity decreased, which also led to a reduction in flow rate. Additionally, the graph displays the change in porosity resulting by leakage of glass beads into the filter. In the case of GB-I, the relatively large pore size ratio d/D_{15}^{s} resulted in more beads passing through the filter and greater porosity reduction.

Figure 16 illustrates the relationship between wire diameter and the quantity of glass beads that moved into the filter. The amount of particle movement was higher for GB-I

due to its smaller particle size. Furthermore, for each bead type, a wire diameter (ϕ) corresponding to the minimum particle movement was identified. These results suggest that the wire diameter should be designed within an appropriate range based on the particle size of the original soil material. Specifically, the following condition is proposed as a suitable standard for wire diameter:

$$5D_{15}^{s} < \phi < 10\,D_{15}^{s} \quad (5)$$

This indicates that the structural stability and permeability performance of 3D filters can be optimized by adjusting wire diameter within this range.

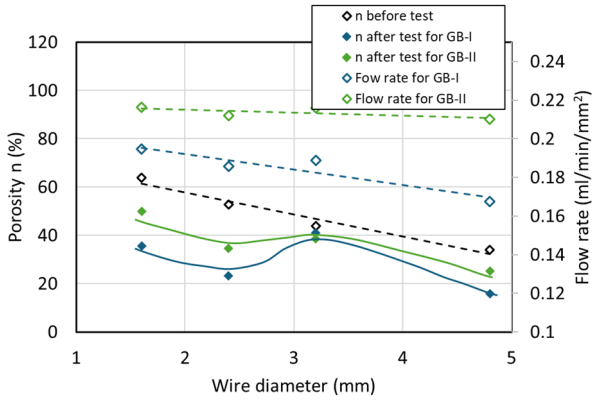

Figure 15. Porosity inside diamond filter and Flow rate plotted against wire diameter.

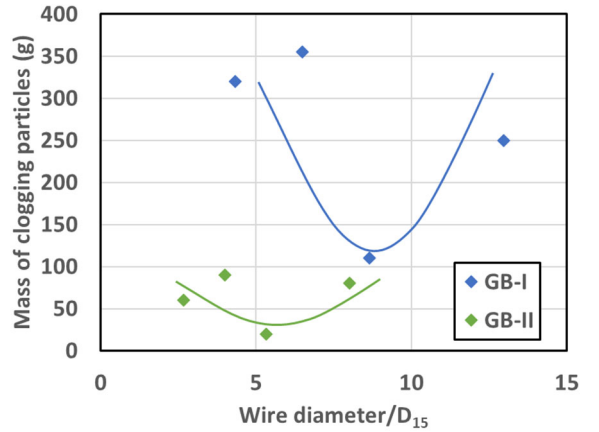

Figure 16. Variation of clogging particles mass in filter on wire diameter.

5 CONCLUSIONS

In light of increasing rainfall intensity and evolving precipitation patterns, the prevention and mitigation of filter clogging has become a critical engineering challenge. This study explored the potential of three-dimensional (3D) structural filters as an effective solution to this problem, given their ability to be custom-designed based on the grain size characteristics of the surrounding ground material.

A series of seepage failure experiments using a small-scale embankment model were conducted to verify the applicability of 3D filters. The results confirmed that the installation of 3D filters as horizontal drainage layers significantly reduced the water head, thereby enhancing slope stability. Among the various types of 3D filters tested, it was found that setting the pore diameter (d) to less than 10 times the D_{15}^{s} of the base soil is effective. This range maintains a balance between minimizing clogging and ensuring adequate permeability.

To establish a standard for wire diameter (ϕ), a one-dimensional infiltration experiment was performed. The movement of soil particles into the filter was used as an indicator of erosion. Based on the extent of particle intrusion, it was determined that the optimal wire diameter lies within the range of 5 to 10 times D_{15}^{s}.

6 ACKNOWLEDGEMENTS

This study is based on the experimental work conducted by Mr. Y. Takata and Ms. M. Yoden during their time as students at Yamaguchi University. The authors would like to express their sincere gratitude to them for their valuable contributions. The authors also gratefully acknowledge the financial support provided by the Japan Society for the Promotion of Science (JSPS) through Grant-in-Aid for Scientific Research (B), 23K22861.

7 REFERENCES

Terzaghi, K. 1926. Effect of Minor Geologic Detail on the Safety of Dams. *American Institute of Mining Engineers*, Technical Publication 215.

Kudai, K., Sassa, S., Yang, S., and Takada, K. 2021. Influence of soil and hydraulic conditions on the processes of internal erosion, cavity formation and collapse behind coastal structures. *Coastal Engineering*, 170, 104013.

Fujiwara Y., Sakai, T., Onabe, T., and Oishi, S. 2020. Verification of effects of seepage water drainage measure in road embankments using crushed-stone ground improvement body and fraining pipes. *Journal of Japan Society of Civil Engineers C*, 76, 1, 40-51.

Schoen, A. H. 1970. Infinite periodic minimal surfaces without self-intersections. *National Aeronautics and Space Administration*, Vol. 5541.

Nguyen-Van, V., Tran, P., Peng, C., Pham, L., Zhang, G., and Nguyen-Xuan, H. 2020. Bioinspired cellular cementitious structures for prefabricated construction: Hybrid design & performance evaluations. *Automation in Construction*, 119, 103324.

Al-Ketan, O., Rowshan, R., and Al-Rub, R. K. A. 2018. Topology-mechanical property relationship of 3D printed strut, skeletal and sheet based periodic metallic cellular materials. *Additive Manufacturing*, 19, 167-183.

Dang, B. L., Nguyen-Van, V., Tran, P., Wahab, M. A., Lee, J., Hackl, K., and Nguyen-Xuan, H. 2022. Mechanical and hydrodynamic characteristics of emerged porous Gyroid breakwaters based on triply periodic minimal surfaces. *Ocean Engineering*, 254, 111392.

Haverkamp R., Parlonge J.Y. 1986. Predicting the water-retention curve from a particle-size distribution 1. Sandy soils without organic matter. *Soil Science*, 142, 325-339.